

THE PROGENITORS OF TYPE IA SUPERNOVA EXPLOSIONS ARE HEAD-ON COLLISIONS OF WHITE DWARFS IN TRIPLE SYSTEMS

DORON KUSHNIR¹, BOAZ KATZ^{1,2}, SUBO DONG¹, ELI LIVNE³, AND RODRIGO FERNÁNDEZ¹

Draft version March 7, 2013

ABSTRACT

We argue that type Ia supernovae (SNe Ia) are the result of head-on collisions of White Dwarfs (WDs) in triple systems. The thermonuclear explosions resulting from the zero-impact-parameter collisions of WDs are calculated from first principles by using 2D hydrodynamical simulations. Collisions of typical WDs with masses $0.5\text{--}0.9M_{\odot}$ result in explosions that synthesize ^{56}Ni masses in the range of $0.15\text{--}0.8M_{\odot}$, spanning the wide distribution of yields observed for the majority of SNe Ia. The robustness of the shock ignition process is verified with a detailed study using a one-dimensional toy model and analytic tools. The late-time ($\gtrsim 50$ days after peak) bolometric light curve is equal to the instantaneous energy deposition and is calculated exactly, by solving the transport of γ -rays emitted by the decay of ^{56}Ni using a Monte-Carlo code. All collisions are found to have the same late-time light curves, when normalized to the amount of synthesized ^{56}Ni . This universal light curve is shown to agree with the majority of the supernovae in the compilation made by M. Stritzinger to an accuracy of better than 30% in the range $40 < t < 80$ days after bolometric peak. The widths of the ^{56}Ni -mass-weighted-line-of-sight velocity distributions are correlated with the ^{56}Ni yield and in agreement with the observed Mazzali relation. The continuous distribution of observed SN Ia features, is naturally reproduced with the distribution of WD masses involved in the collisions. The effect of a non-zero impact parameter requires further studies, using 3D hydrodynamical codes.

Subject headings: hydrodynamics – shock waves – supernovae: individual (Ia)

The explosion mechanism of carbon-oxygen white dwarfs (CO WDs) to produce type Ia SNe is unknown (see Hillebrandt & Niemeyer 2000, for a review). It is widely thought that the explosion is mediated by accretion of matter onto the WD. As it approaches the Chandrasekhar mass, an unknown process is believed to ignite a nuclear detonation. The observed light curve is known to be powered by ^{56}Ni synthesized in the explosion through the radioactive decay chain $^{56}\text{Ni} \rightarrow ^{56}\text{Co} \rightarrow ^{56}\text{Fe}$.

Katz & Dong (2012) suggested that some or all of SNe Ia arise from head-on collisions of typical field WDs in triple systems. In this scenario, the nuclear detonation is due to a shock ignition and is not related to whether or not the total mass of the colliding WDs is above or below the Chandrasekhar limit. In fact, most WDs have masses peaked around $0.6M_{\odot}$, and most collisions are expected to have a total mass of $1.2M_{\odot}$, well below that limit. While Katz & Dong (2012) showed that the rate of such collisions may be as high as the rate of SNe Ia, it is unclear whether such collisions actually lead to explosions having the same observational properties as SNe Ia.

Calculations of the thermonuclear explosion of colliding WDs was attempted by several groups (Benz et al. 1989; Raskin et al. 2009; Rosswog et al. 2009; Lorén-Aguilar et al. 2010; Raskin et al. 2010; Hawley et al. 2012), using 3D hydrodynamic simulations, motivated by the prospects of detecting rare SNe Ia in the cores of dense globular clusters. While the amount of ^{56}Ni synthesized in most of these simulations was non negligible, the results were contradictory, yielding different amounts of ^{56}Ni . Furthermore, the ignition

site (contact region or shock region) is different between the different calculations for the same initial conditions.

We use numerical simulations to calculate, from first principles, the explosion that is obtained from zero-impact parameter collisions of CO WDs with masses $0.5, 0.6, 0.7, 0.8, 0.9M_{\odot}$, covering the range of WD masses, including various equal and non-equal mass combinations. This problem is axis-symmetric, allowing the use of 2D numerical simulations, with high resolution (\sim few km cell size) that greatly supersede previous Eulerian approaches (limited to > 100 km cell sizes) by Hawley et al. (2012). The cell volumes of our 2D calculations are smaller than the volumes of the particles in the SPH runs (particle mass divided by the highest density) by Raskin et al. (2010). Furthermore, we employ 1D planar toy models (see Figures 2 and 3) to ensure that the ignition process, in the 2D simulation (see Figure 1) is correctly resolved based on the fact that the curvature of the shock has little effect on the ignition process, which is largely a 1D problem. Moreover, we used two different 2D codes, Eulerian adaptive mesh refinement FLASH4.0 (Dubey et al. 2009) and Arbitrary Eulerian Lagrangian (ALE) code VULCAN2D (for details, see Livne 1993), which yield the same ^{56}Ni mass and the same location of detonation ignition.

Numerical unstable burning occurs if the energy in a cell is significantly increased in a time shorter than the sound crossing time, $t_s \equiv \Delta x/c_s$, where Δx is the length scale of the cell and c_s is the speed of sound. This is avoided by limiting the energy injection rate from burning, \dot{Q} , to $0.1\varepsilon/t_s$, where ε is the internal energy of the numerical cell. This is implemented by appropriate renormalization of all burning rates within a cell if the limit is superseded. As the numerical resolution increases the renormalization becomes less severe, guaranteeing correct convergence while avoiding premature ignition. We emphasize that the limiter does not modify the induction time, which is set at lower temperatures, where the stabil-

¹ Institute for Advanced Study, Einstein Drive, Princeton, New Jersey, 08540, USA

² John N. Bahcall Fellow, Einstein Fellow

³ Racah Institute of Physics, Hebrew University, Jerusalem, Israel

ity criterion is automatically satisfied. Therefore, the limiter does not modify the ignition process. Correct convergence is conformed by the calculations performed with the ALE code, VULCAN2D, which did not require the use of a limiter at sufficiently high resolution (see upper panel of Figure 3). Previous Eulerian calculations, which violated this numerical stability criterion, erroneously ignited too early at the contact region for several scenarios (Hawley et al. 2012), where they should have ignited later at the shock region. This is the main reason for the reported contradiction between the SPH and the Eulerian codes. In our calculations, collisions involving low mass WDs ($\lesssim 0.7$) ignite at the shock region, while higher mass WDs ignite at the contact region, in agreement with the SPH simulations (Rosswog et al. 2009; Raskin et al. 2010).

The amount of ^{56}Ni , synthesized in the various collisions is provided in Table 1, and shown in Figure 4. The collisions of typical CO WDs in the mass range $0.5 - 1 M_{\odot}$ produce ^{56}Ni masses in the range $0.1 - 1 M_{\odot}$ in agreement with inferred range of SNe Ia, and thus provides a natural explanation for these SNe. This is the main result of this paper.

A comprehensive comparison of the observational features of SNe to the collision model requires a detailed modeling of the complicated radiation transfer of optical light and is beyond the scope of this paper. Next, we show that the model succeeds in satisfying two non-trivial, robust observational tests, which are independent of the optical radiation transfer details, and allow a direct comparison of the model to the observations.

The late time ($\gtrsim 50$ days after peak) bolometric luminosity equals the total instantaneous γ -ray energy deposition rate, which is calculated exactly from first principles, by numerically solving the transport of γ -rays, which is dominated by Compton scatterings. We find that the escaping fraction of γ -rays as a function of time is the same in all of our models, and agrees with each of the 24, low extinction (Galactic+host $E(B-V) < 0.3$), $L_{\text{bol}}/M^{56}\text{Ni}$ observed in the sample of bolometric light curves compiled by Stritzinger et al. (2005) (see Figures 5-6). For illustration, the light curve of a simple Chandrasekhar toy model, with an exponential distribution of density ($\rho \propto e^{-v}$) is shown. As can be seen, for ^{56}Ni mass of $0.15 M_{\odot}$ (observed in some SNe), the Chandrasekhar light curve is higher than that from our model and also higher than the observations. This is due to the high optical depth of the massive $1.25 M_{\odot}$ ejecta surrounding the ^{56}Ni . This ejecta is moving slightly slower (by $\sim 10\%$) than that of the higher, $0.8 M_{\odot}$, ^{56}Ni models due to the lower amount of nuclear energy released, and this leads to an additional $\sim 20\%$ increase in γ -ray deposition.

The distribution of widths of the (^{56}Ni mass weighted) line of sight velocities for the collision models is compared to the widths inferred from nebular phase observations of SNe Ia in Figure 7. The model widths (v_{mod}) are obtained by fitting the LOS velocity distributions using a quadratic distribution ($dM^{56}\text{Ni}/dN \propto 1 - v^2/v_{\text{mod}}^2$) commonly used and equivalent to homogenous expansion. The observational widths are obtained by fitting the spectra in the range 4800–5700 Å using the narrow spectra of 1991bg and 1999by as templates, by assuming local emission with a quadratic distribution of velocities. The amount of ^{56}Ni in the SNe is obtained by fitting intermediate bolometric light curves ($t \sim 60$ day) to the universal injection function presented in Figure 5, which is well described by $L_{\text{deposit}} = (1 + (t_d/40)^3)^{-2/3} L_{\text{decay}}$, where t_d is the time from explosion in days and L_{decay} is the energy released

in γ -rays by ^{56}Ni and ^{56}Co . As can be seen, there is a clear correlation between the observed ^{56}Ni and the nebular phase velocity widths. This Mazzali relation (Mazzali et al. 1998) is well reproduced by the collision model. The amount of SNe with nebular spectra and well described bolometric light curves is limited. In the top panel larger samples of SNe are used to show the continuous correlation of observational features of SNe Ia with ^{56}Ni yields. The strong correlation between ^{56}Ni yields and WD mass in the collision model, Figure 4, is suggestive as the source for these correlations, including possibly the Phillips relation (Phillips 1993). In fact, Phillips (1993) had suggested a varying progenitor mass as a natural source for the relation.

We emphasize that there are likely numerous detailed comparisons of our calculations to observations. One very robust and detailed prediction is the time dependent gamma-ray spectrum which can be calculated in a straight forward manner given the precisely known process of Compton scattering. While such observations may be very powerful, it is unclear when such observations will be available. Other directions which are closely related to the nebular velocity widths reported here, include the distribution of non-zero nebular line shifts, which are expected in the collision of non-equal mass WDs, as well as the unique line shapes resulting from the non-trivial velocity distribution in many of the collision scenarios.

SNe Ia are used as standard candles, under the assumption that they would have no systematic change due to chemical evolution of the galaxy and physical evolution of the star-formation process, without any firm theoretical basis. Now for the first time we have a precise theory that allows us to calculate systematic changes if they exist, and the differences between ancient and modern SNe can be reliably estimated.

The authors thank R. Kirshner, J. Prieto, M. Zaldarriaga, and F. Dyson for useful discussions, and thank A. Gould for carefully reading the manuscript. D. K., S. D., and R. F. are supported by NSF grant AST-0807444. B. K. is supported by NASA through the Einstein Postdoctoral Fellowship awarded by Chandra X-ray Center, which is operated by the Smithsonian Astrophysical Observatory for NASA under contract NAS8-03060. S. D. was supported through a Ralph E. and Doris M. Hansmann Membership at the IAS. The software FLASH used in this work was in part developed by the DOE NNSA-ASC OASCR Flash Center at the University of Chicago. We thank the Princeton Institute for Computational Science and Engineering (PICSciE) and the Office of Information Technology's High Performance Computing Center and Visualization Laboratory at Princeton University for access to their computational resources. Computations were performed at the Princeton Hecate and IAS Aurora clusters.

REFERENCES

- Benz, W., Thielemann, F.-K., & Hills, J. G. 1989, *ApJ*, 342, 986
- Blondin, S., Matheson, T., Kirshner, R. P., et al. 2012, *AJ*, 143, 126
- Dubey, A., Reid, L. B., Weide, K., et al. 2009, arXiv:0903.4875
- Hawley, W. P., Athanassiadou, T., & Timmes, F. X. 2012, *ApJ*, 759, 39
- Hillebrandt, W., & Niemeyer, J. C. 2000, *ARA&A*, 38, 191
- Katz, B., & Dong, S. 2012, arXiv:1211.4584
- Katz, B., Kushnir, D., & Dong, S. 2013, arXiv:1301.6766
- Livne, E. 1993, *ApJ*, 412, 634
- Lorén-Aguilar, P., Isern, J., & García-Berro, E. 2010, *MNRAS*, 406, 2749
- Mazzali, P. A., Cappellaro, E., Danziger, I. J., Turatto, M., & Benetti, S. 1998, *ApJ*, 499, L49
- Phillips, M. M. 1993, *ApJ*, 413, L105

- Raskin, C., Timmes, F. X., Scannapieco, E., Diehl, S., & Fryer, C. 2009, MNRAS, 399, L156
- Raskin, C., Scannapieco, E., Rockefeller, G., et al. 2010, ApJ, 724, 111
- Rosswog, S., Kasen, D., Guillochon, J., & Ramirez-Ruiz, E. 2009, ApJ, 705, L128
- Silverman, J. M., Ganeshalingam, M., & Filippenko, A. V. 2013, MNRAS, 430, 1030
- Stritzinger, M., 2005, Phd thesis submitted to the Max Planck Institute for Astrophysics,
- Zeldovich, Ya B, 1980, Combustion and Flame, 39, 2, 211

Table 1

Summary of the results of the numerical simulations with FLASH, for the high resolution runs. Columns 1,2: The masses of the WDs (M_1 is the more massive WD); Column 3: the size of cells in the highest refinement level (we use 7 levels of refinement for these runs); Column 4: The type of ignition obtained in the simulation: for equal mass collisions the ignition is either at the shock region (s) or at the contact region (c). For non-equal mass collisions, the less massive star always ignites first, either near the shock region (s2) or near the contact region (c2), followed either by an ignition of the more massive star at the shock region (s1) or no second ignition (x1); Column 5: The mass of ^{56}Ni synthesized in the explosion; Column 6: The total energy of the ejecta.

$M_1 [M_\odot]$	$M_2 [M_\odot]$	$\Delta x [\text{km}]$	Ignition type	^{56}Ni mass [M_\odot]	$E_{\text{tot}} [10^{51} \text{ erg}]$
0.5	0.5	9.5	s	0.10	0.94
0.55	0.55	9.0	s	0.19	1.17
0.6	0.5	9.5	s2,s1	0.19	1.17
0.6	0.6	8.5	s	0.29	1.32
0.64	0.64	8.1	s	0.37	1.46
0.7	0.5	9.5	c2,s1	0.27	1.19
0.7	0.6	8.5	s2,s1	0.44	1.48
0.7	0.7	7.6	s	0.50	1.66
0.8	0.5	9.5	c2,x1	0.28	1.14
0.8	0.6	8.5	c2,s1	0.36	1.41
0.8	0.7	7.6	c2,s1	0.52	1.67
0.8	0.8	6.8	c	0.73	1.93
0.9	0.5	9.5	c2,s1	0.64	1.49
0.9	0.6	8.5	c2,x1	0.52	1.53
0.9	0.7	7.6	c2,s1	0.48	1.70
0.9	0.8	6.8	c2,s1	0.72	1.96
0.9	0.9	6.1	c	0.76	2.12
1.0	0.8	6.8	c2,x1	0.89	2.04
1.0	1.0	5.3	c	1.25	2.45

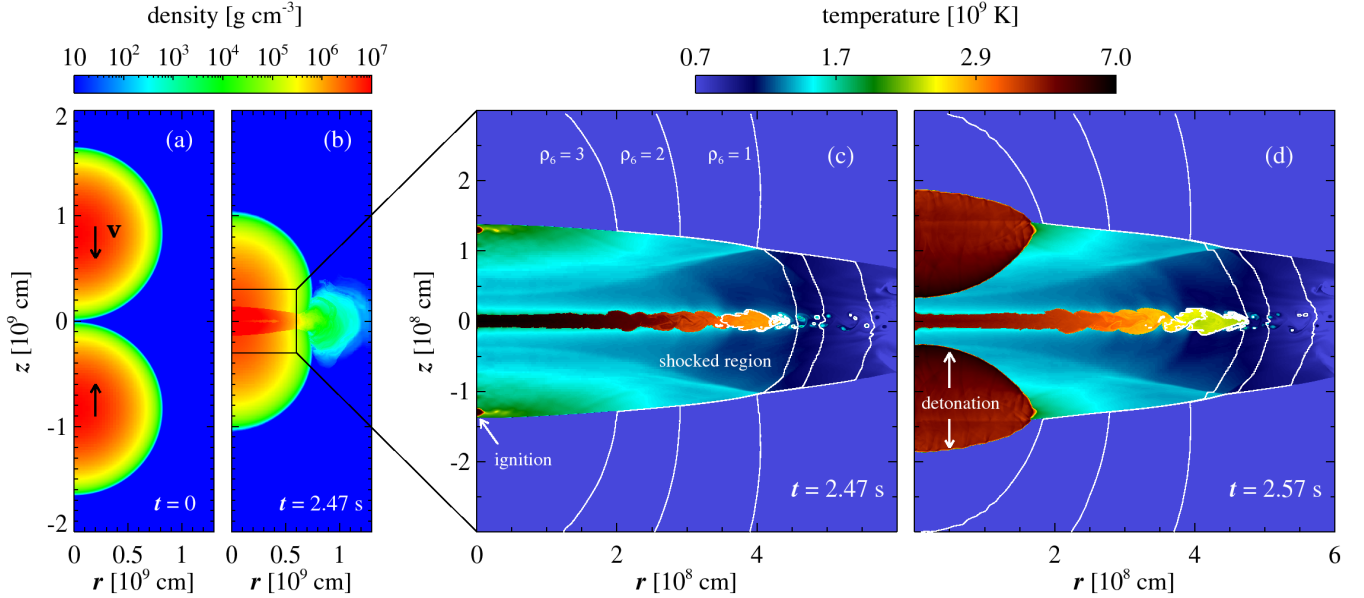


Figure 1. The shock ignition process is illustrated using snapshots from the numerical calculation of a $0.64-0.64 M_\odot$ collision done with FLASH with numerical resolution of $\approx 4 \text{ km}$. In panel (a) a logarithmic density map of the initial conditions of the calculation is shown. The black arrows indicate the direction of the velocity (assumed uniform) of each star. Following contact, a shock wave propagates from the contact surface toward the center of each star. The shock accelerates, leading to an increasing post shock temperature and rapidly increasing burning rates. Ignition of the detonation occurs once the induction time is shorter than the timescale for significant increase in burning rate (Zeldovich 1980). Panel (b) shows a density map at the time of ignition at the shock front ($t = 2.47 \text{ s}$). Two detonation waves begin to propagate from the ignition point, one inward and one outward. This process is fully resolved in our calculations, and the two ignition sites (one in each star) are clearly seen. The propagating detonation waves are evident in panel (d), which shows the same temperature map at a slightly later time, $t = 2.57 \text{ s}$. Note that the mass surface where the ignition occurs becomes a contact discontinuity which is clearly seen in panel (d). An interesting feature seen in panels (c)-(d) is the outgoing jet, originating at the contact surface. This (planar) jet arises due to the high pressures obtained at contact, which are not counter balanced from the outside.

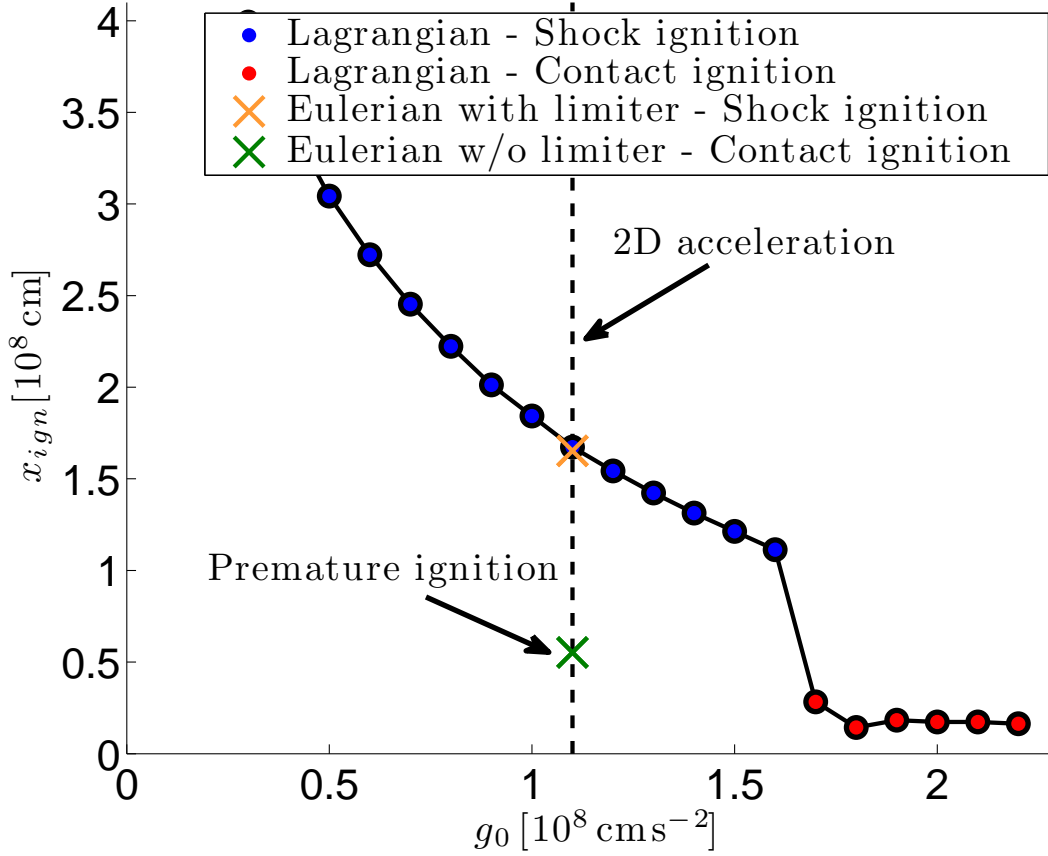


Figure 2. The ignition process shown in Figure 1 is confirmed using a planar 1D toy model evolved with Lagrangian and Eulerian schemes. This is possible since the hydrodynamical flow near the symmetry axis of the problem, where the ignition occurs, has approximate planar symmetry. The model consists of two equal mass WDs, with an initial planar density equal to the density on the axis of symmetry in the 2D model at the same distance from the contact surface. The gravitational field is mimicked by an adjustable constant acceleration (in time and space). In order to avoid artificial rapid early expansion due to the non physical tidal field, each mass element is forced by hand to fall at the constant external acceleration, until the point in time at which it is first shocked. The converged location of the ignition x_{ign} , obtained with a high resolution Lagrangian scheme is shown as a function of the adjustable acceleration, g_0 : filled blue dots (shock region ignition) and red dots (contact region ignition). Beyond a critical acceleration of about $1.6 \times 10^8 \text{ cm s}^{-2}$ the detonation occurs in the contact region. The acceleration $g_0 \approx 1.1 \times 10^8$, shown as a dashed line, approximately reproduces the 2D velocity profiles in Figure 1. The burning in the Eulerian code with resolution $\Delta x \sim \text{few km}$ is unstable (see text), and leads to a premature detonation at the contact region (green cross) unless the burning is limited to be slower than the cell crossing time. The Eulerian scheme reproduces the correct ignition location when the limiter is included (orange cross).

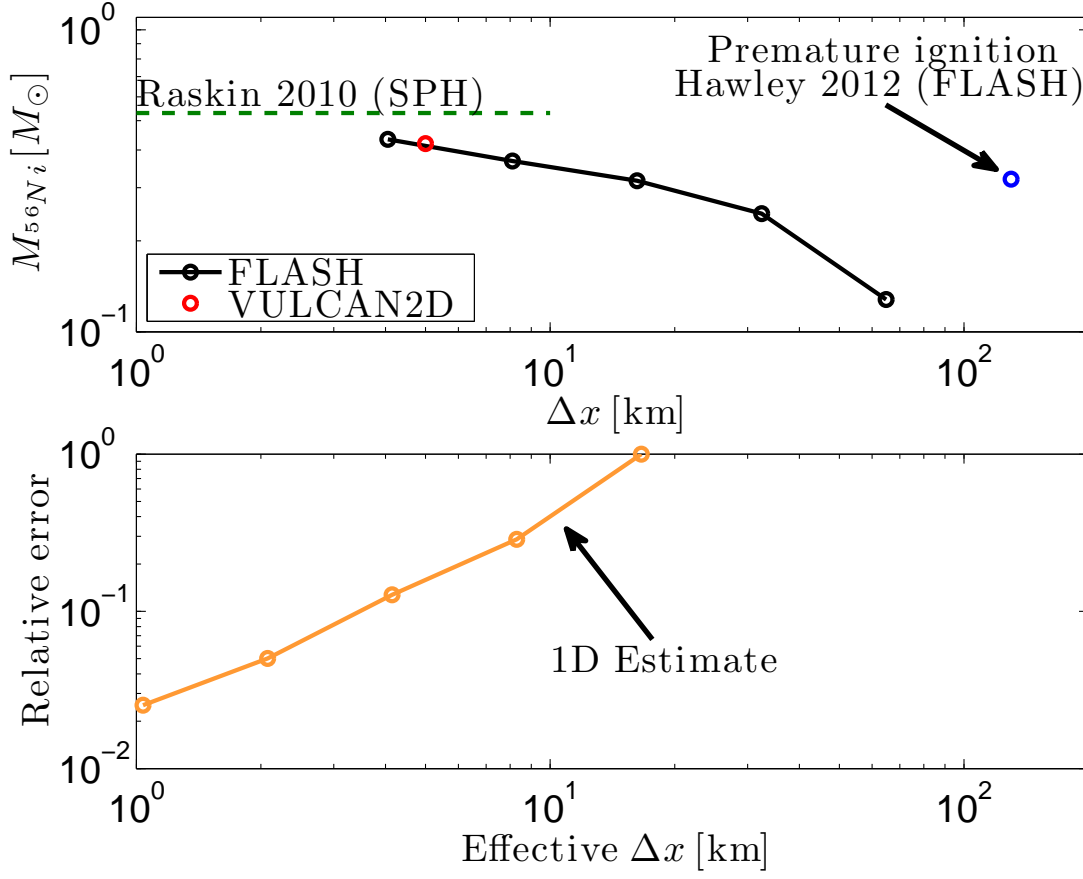


Figure 3. The convergence of the ^{56}Ni mass as a function of resolution in our Eulerian 2D FLASH model is shown in black circles for the $0.64 - 0.64 M_\odot$ collision simulation. The ALE VULCAN2D code (red circle) reproduces the same value when compared at the same resolution. Our results are consistent with the SPH calculation performed by Raskin et al. (2010). In the Eulerian calculation performed by Hawley et al. (2012), premature ignition at the contact surface occurs (blue point, see also Figure 2), due to burning which is faster than the cell sound crossing time. In the lower panel we show the decreasing error in the ^{56}Ni yield as a function of resolution in the 1D Eulerian model. Based on the 1D run, we estimate that the ^{56}Ni yield in our highest resolution FLASH run (maximum level of refinement 8), is converged to about 10%. All other scenarios were calculated with lower maximum level of refinement 7, for which the ^{56}Ni masses are converged to about 20–30% accuracy (higher mass WDs have smaller radii and convergence is more easily obtained due to the smaller cell sizes for a given level of refinement).

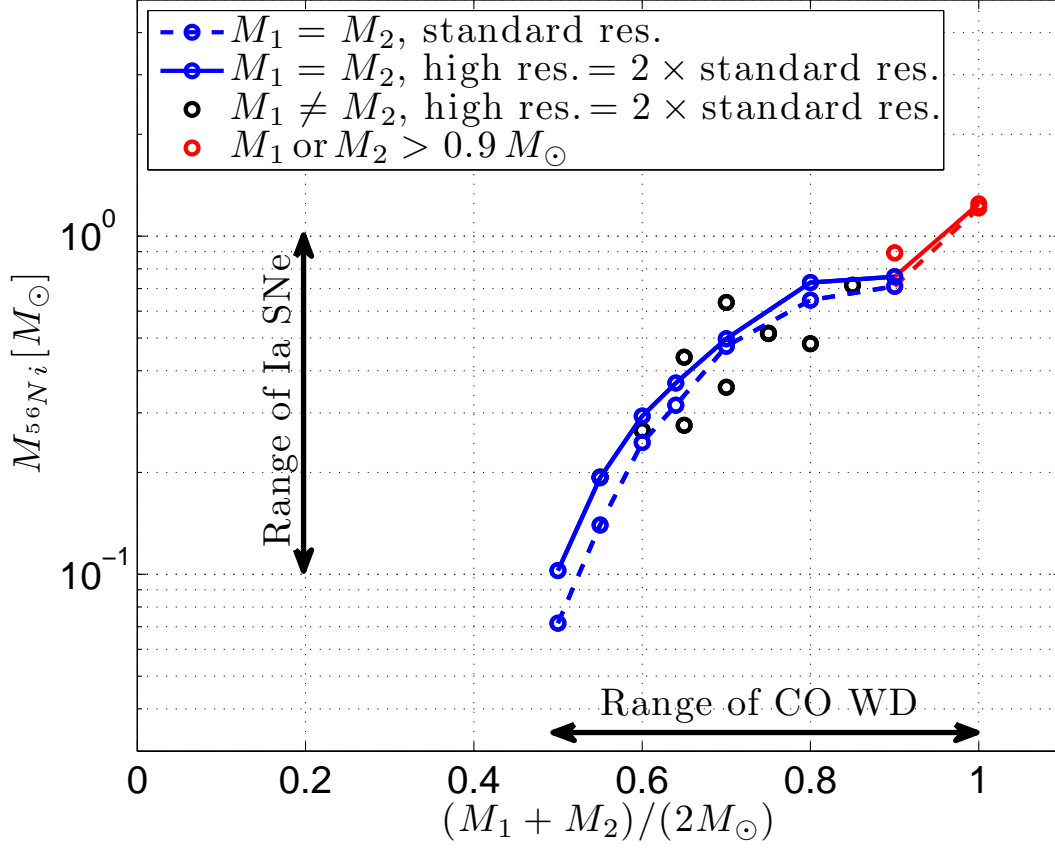


Figure 4. The amount of ^{56}Ni synthesized in the numerical collisions is shown as a function of the mean mass of the colliding WDs at two resolutions and for equal and non-equal mass collisions. As can be seen, the yield function is converged and collisions of CO white dwarfs lead to the synthesis of $\sim 0.1 - 1 M_\odot$ of ^{56}Ni covering the range of yields observed in the vast majority of SNe Ia. This is the main result of this paper.

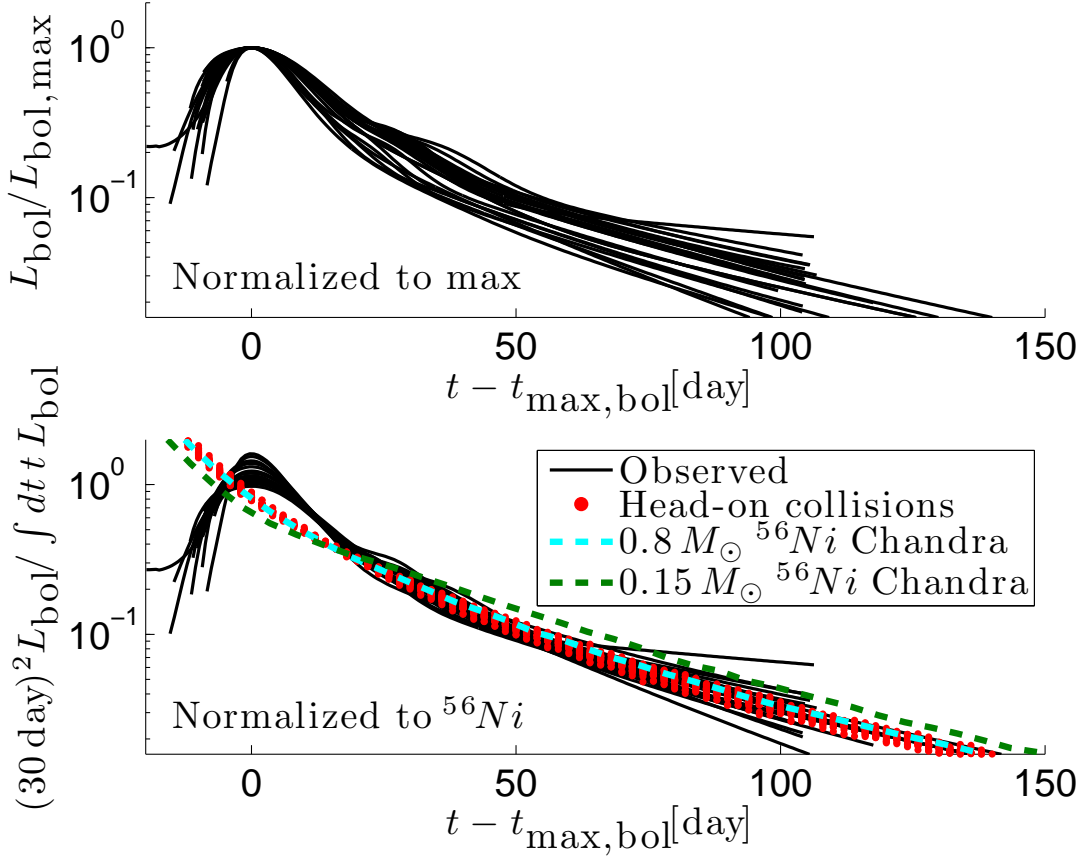


Figure 5. Normalized bolometric light curves (black solid lines) of 24 SNe Ia, from the sample compiled by Stritzinger et al. (2005). Panel a: Bolometric luminosity normalized to the peak luminosity. Panel b: Bolometric luminosity, normalized by the (time weighted) integrated luminosity, $\int dt t L(t)$, which is proportional to the ^{56}Ni yield (Katz et al. 2013). The integral is performed to 80 days after the explosion, and the time of explosion is assumed to be 19 days prior to maximum. The instantaneous energy deposition by γ -rays in the expanding ejecta for all the collision models are shown (red dots), calculated using an exact Monte Carlo code, normalized by their time-weighted integral. At late times $\gtrsim 40$ day, the diffusion of optical radiation is short and this injected bolometric luminosity equals the emitted bolometric luminosity. The late time luminosity of the models is in excellent agreement with the observed light curves (see also a close up view in Figure 6). The late time luminosity calculated from a simple Chandrasekhar model with ^{56}Ni yields of $0.8 M_{\odot}$ (cyan dashed) and $0.15 M_{\odot}$ (green dashed) is shown for comparison to illustrate that this agreement is far from trivial. Note that a much larger scatter is obtained when the light curves are normalized to the peak luminosity which is not directly proportional to the ^{56}Ni yield, as commonly believed.

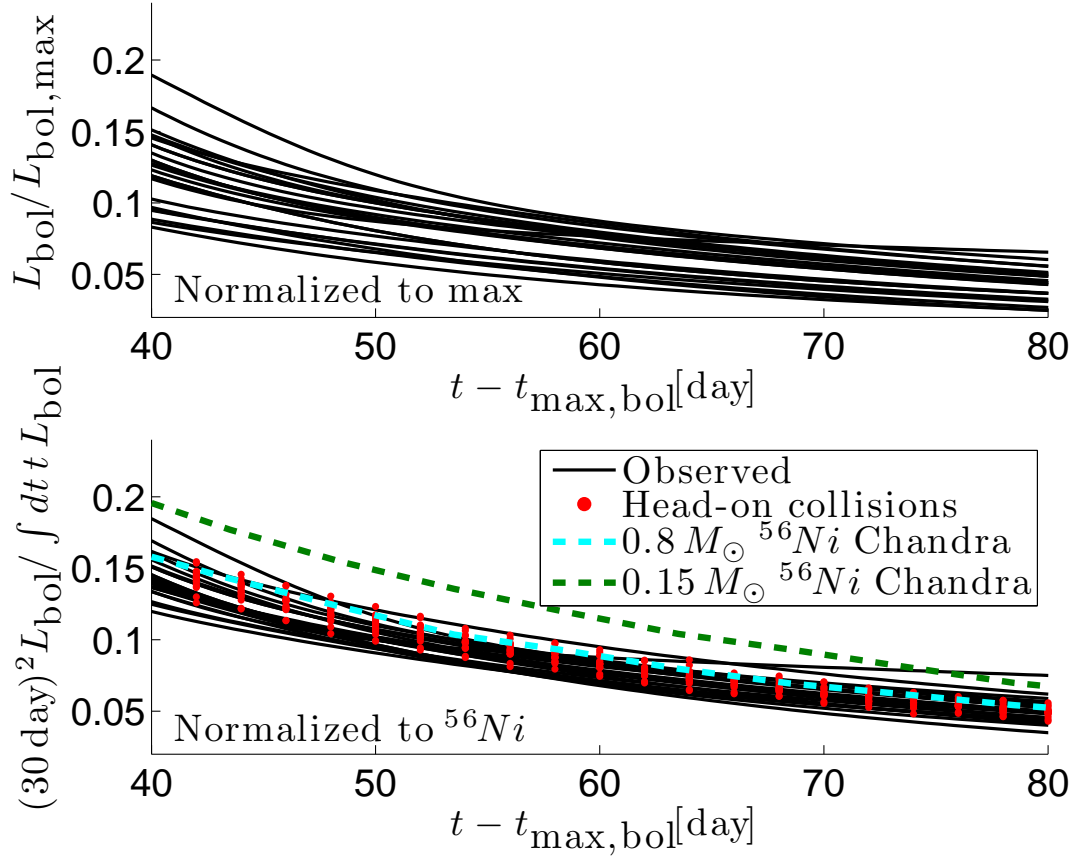


Figure 6. Close up view of the bolometric light curves from Figure 5

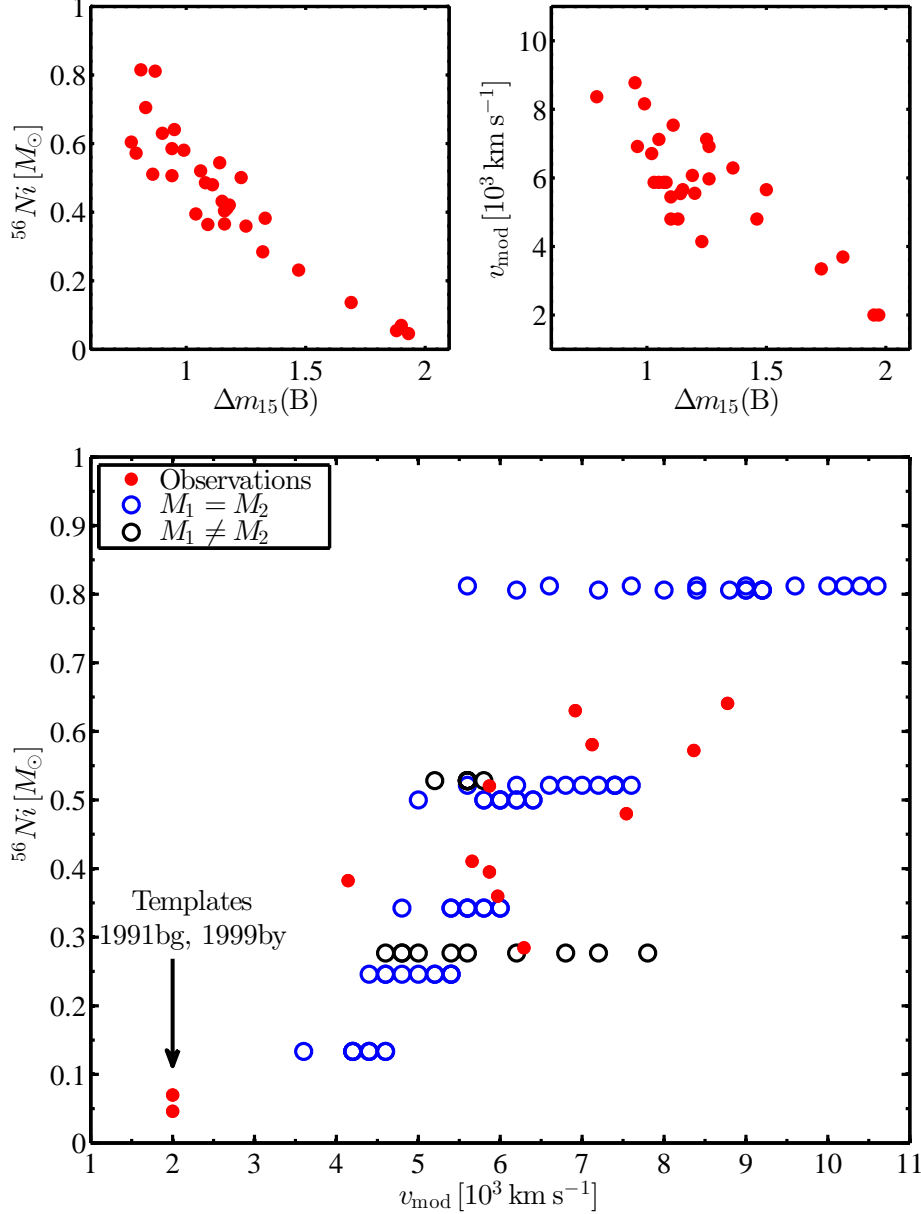


Figure 7. Bottom panel: Widths of the (^{56}Ni weighted) line of sight (LOS) velocity distribution from the collision models (empty circles) compared to the widths inferred from nebular phase observations of SNe Ia (red points). Late time (>150 days) spectra are obtained from the Berkeley Supernova Ia Program (BSNIP) (Silverman et al. 2013), the Center for Astrophysics Supernova Program (Blondin et al. 2012), and the compilation from various sources by the Online Supernova Spectrum Archive (SUSPECT, <http://suspect.nhn.ou.edu/~suspect/>). The model widths (v_{mod}) are obtained by fitting the LOS velocity distributions using a quadratic distribution ($dM_{^{56}\text{Ni}}/dN \propto 1 - v^2/v_{\text{mod}}^2$) commonly used and equivalent to an homologous expansion. The observational widths are obtained by fitting the spectra in the range 4800–5700 Å using the narrow spectra of 1991bg and 1999by as templates, by assuming local emission with a quadratic distribution of velocities. The amount of ^{56}Ni in the SNe is obtained by fitting intermediate bolometric light curves ($t_d \sim 60$ day) to the universal injection function presented in Figure 5, which is well described by $L_{\text{deposit}} = (1 + (t_d/40)^3)^{-2/3} L_{\text{decay}}$, where t_d is the time from explosion in days and L_{decay} is the energy released in γ -rays by ^{56}Ni and ^{56}Co . As can be seen, there is a clear correlation between the observed ^{56}Ni and the nebular phase velocity widths. This so-called Mazzali relation (Mazzali et al. 1998), is well reproduced by the collision model. The number of SNe with nebular spectra and well described bolometric light curves is limited. In the top panel larger samples of SNe are used to show the continuous correlation of observational features of SNe Ia with ^{56}Ni yields. The strong correlation between ^{56}Ni yields and WD mass in the collision model, Figure 4, is suggestive as the source for these correlations, including possibly the Phillips relation (Phillips 1993). In fact, Phillips (1993) had suggested a varying progenitor mass as a natural source for the relation.